Sensors & Actuators: B. Chemical 276 (2018) 413–420

Contents lists available at ScienceDirect

Sensors and Actuators B: Chemical

journal homepage: www.elsevier.com/locate/snb

Facile synthesis of La-doped In_2O_3 hollow microspheres and enhanced hydrogen sulfide sensing characteristics

Dongdong Wei, Wenhao Jiang, Hongyu Gao, Xiaohong Chuai*, Fengmin Liu, Fangmeng Liu, Peng Sun, Xishuang Liang, Yuan Gao, Xu Yan, Geyu Lu*

State Key Laboratory on Integrated Optoelectronics, Jilin Province Key Laboratory on Advanced Gas Sensors, College of Electronic Science and Engineering, Jilin University, 2699 Qianjin Street, Changchun 130012, People's Republic of China

ARTICLE INFO

Keywords:
Hydrothermal
La-doped In_2O_3
Hollow microspheres structures
Hydrogen sulfide sensor

ABSTRACT

The undoped and 1.0–5.0 mol% La–doped In_2O_3 hollow microspheres have been successfully synthesized via a simple hydrothermal method without template and gas sensor have been fabricated basing on them. The nanostructures and morphologies of the maintained hollow spheres were characterized by various experimental techniques. The gas sensing properties of these hollow microspheres were investigated systematically. The results indicated that among all the samples (pure, 1.0, 3.0 and 5.0 mol% La–doped In_2O_3), 3.0 mol% La–doped In_2O_3 exhibited the highest response toward 10 ppm hydrogen sulfide (H_2S) at 200 °C, having a response value of 17.8, approximately 4.8 times higher than pure In_2O_3. Furthermore, excellent selectivity, good repeatability and outstanding long-term stability were also achieved. The significantly enhanced sensing properties to H_2S could be attributed to the changes in distribution of different oxygen components, crystallite size and specific surface area caused by La doping.

1. Introduction

In recent years, the monitoring of toxic gases is becoming more and more important to humans safety and environment protection. Hydrogen sulfide (H_2S) is a colorless, flammable acid gas with a stench of rotten eggs at low concentrations, while at high concentrations, it could paralyze the human olfactory nerve, causing it is odorless. Hydrogen sulfide is a highly toxic substance, even small amounts of high-concentration sulfide can be fatal to human in a short period of time [1–6]. Low concentrations of hydrogen sulfide also have an adverse impact on human eyes, respiratory and central nervous. Up to now, several methods have been used for the detection of H_2S, including solid electrolytes [7,8], organic films [9,10] and metal oxide semiconductors [11,12]. Among them, metal oxide semiconductor sensors are widely researched because of their marked advantages of low cost, high sensitivity, fast response and simple manufacturing. However, some disadvantages still exist to putting the sensors into practical application eventually. Especially, it is uneasy for the resistances of sensors to recover to their initial values when H_2S gas is removed during the process of gas testing [13]. Thus, it needs to be tested under high temperature to restore its resistance owing to the fast desorption for H_2S gas.

In the past few decades, researchers have widely investigated various oxide semiconductors to detect H_2S gas, including CuO [14,15], SnO_2 [16,17], α-Fe_2O_3 [18,19], WO_3 [20,21], In_2O_3 [22,23] and so on. Indium (III) oxide (In_2O_3), as an n-type direct band semiconductor (Eg = 2.8 eV), has been recognized as a suitable gas sensing material due to its high conductivity and abundant defects on the sensing surface. These properties made In_2O_3 become a promising sensing material for H_2S gas sensor. As is known to all, the properties of the nanomaterial are strongly dependent on its morphology, various methods have been used to synthesize In_2O_3 nanostructures with different dimensionals and morphologies, such as nanoparticals [24,25], nanowires [26,27], nanorods [28,29], nanosheets [30,31] and nanospheres [32,33]. Among them, hollow microspheres synthesized by one step hydrothermal method have been demonstrated to have great potential in the application of gas sensor owing to their high specific surface area and high gas accessibility [34,35].

Furthermore, it is well known that the principle of the resistance gas sensor was based on the change of charge carrier caused by surface gas-solid interaction. In view of this, the modulation of charge carrier concentration by doping should be an effective way to improve the H_2S gas sensitivity [36]. For example, Hu et al. reported Pd-doped CuO with nanoflower structure could have higher sensitivity than the undoped

* Corresponding authors.
E-mail addresses: xhchuai@jlu.edu.cn (X. Chuai), lugy@jlu.edu.cn (G. Lu).

https://doi.org/10.1016/j.snb.2018.08.130
Received 22 March 2018; Received in revised form 12 July 2018; Accepted 25 August 2018
Available online 27 August 2018
0925-4005/

one to 50 ppm H_2S at 80 °C [37]. Cu-doped SnO_2 nanospheres were studied by Shu et al. and the sensitivity increases 7 times for the detection of 50-ppm of H_2S at room temperature [38]. Sukunta et al. demonstrated that 0.1%wt V-doped SnO_2 films could exhibited a very high response with a short response time of 2.0 s to 10 ppm of H_2S at 350 °C [39]. These results showed that doping is a promising method to modify In_2O_3 nanomaterial for enhancing its gas sensing performance. Lanthanum oxide (La_2O_3) have been known as catalysts in many fields. As for gas sensor, La_2O_3 doping has been used to improve both selectivity and sensitivity of the sensing materials to several gases, such as acetone, H_2S and so on [40–43]. However, as far as we know, the H_2S sensing properties of La–doped In_2O_3 hollow spheres have been barely investigated.

In this work, a simple hydrothermal method was adopted to synthesize the undoped and La–doped In_2O_3 hollow microspheres with great specific area. Meanwhile, several kinds of characterizations were carried out to obtain the crystal structural and morphological information. In addition, the gas sensing properties of synthesized simples were also been examined. According to the results, the sensor with 3.0 mol% La–doped In_2O_3 hollow microspheres exhibited the highest response toward 10 ppm H_2S at 200 °C, having a response value of 17.8, which was about 4.8 times higher than pure In_2O_3. Notablely, there was a clear improvement of response velocity between the 3.0 mol% La–doped and pure In_2O_3 with the response times of 43 s and 178 s, respectively. Besides, excellent selectivity, good repeatability and outstanding long-term stability were also achieved. In the end, the related mechanisms of gas sensing were investigated and discussed.

2. Experimental

2.1. Preparation of pure and La–doped In_2O_3 hollow microspheres

All of the chemical reagents involved in the experiment were analytical grade used as received without further purification. Purchased from Sinopharm Chemical Reagent Co. Ltd. $In(NO_3)_3{\cdot}4.5H_2O$ and $La(NO_3)_3{\cdot}nH_2O$ were used as Indium and Lanthanum sources, respectively.

The pure and La–doped In_2O_3 hollow microspheres with various doping concentrations of 1.0, 3.0 and 5.0 mol% (labeled as S1, S2, S3 and S4, respectively) were synthesized by hydrothermal. In a typical experiment process, 0.26 g (0.68 mmol) of $In(NO_3)_3{\cdot}4.5H_2O$, a certain amount of $La(NO_3)_3{\cdot}nH_2O$ (in a ratio of 1.0,3.0 and 5.0 mol% respectively), 0.50 g of urea were added to the solution of 32 mL absolute alcohol and 3 mL polyethylene glycol (the molecular weight is 400) under vigorous magnetically stirring for 90 min. Then, the homogeneous and transparent solution was transferred into a Teflon-lined stainless-steel autoclave, tightly sealed and maintained at 160 °C for 12 h at the oven. After being cooled to room temperature naturally, the white precipitates were collected and washed by centrifugation with distilled water and absolute alcohol for several times. The final light yellow products were obtained after sintering the white powders at 500 °C for 2 h in air.

2.2. Characterization

The X-ray diffraction (XRD) patterns were recorded by Rigaku TTRIII X-ray diffractometer with Cu K radiation at a wavelength of 1.5406 Å at 40 kV and 200 mA. The field emission scanning electron microscopy (FESEM) images were collected by a JEOL JSM-7500F microscope at an acceleration voltage of 15 kV. The energy dispersive X-ray spectroscopic (EDS) elemental mapping was investigated by the TEM attachment. The transmission electron microscopic (TEM) and high resolution transmission electron microscopic (HRTEM) images, and selected area electron diffractive (SAED) patterns were obtained on a JEOL JEM-2200FS transmission electron microscope at an operating voltage of 200 kV. The X-ray photoelectron spectroscopy (XPS) analysis was conducted on an ESCALABMKII X-ray photoelectron spectrometer with Mg-K 1253.6 eV) achromatic X-ray source. The specific surface area was estimated from the Brunauer–Emmett–Teller (BET) measurements by using a Micromeritics Gemini VII apparatus (Surface Area and Porosity System).

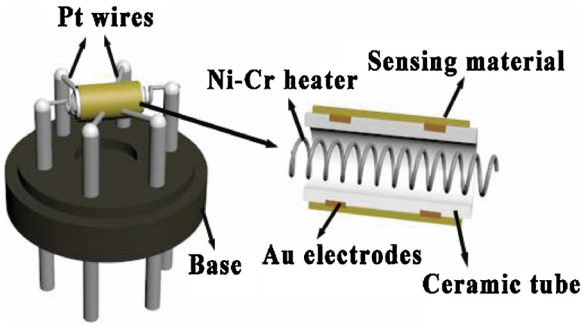

Fig. 1. Schematic diagram of the gas sensor.

2.3. Fabrication and measurement of gas sensor

The schematic structure of the fabricated gas sensor was shown in Fig. 1. Its fabrication process was as follows: The products were mixed with deionized water at a weight ratio of 5:1 to form a paste, and then coated it on the outside of an alumina tube (4 mm in length, 1.2 mm in external diameter, and 0.8 mm in internal diameter, attached with a pair of gold electrodes and each electrode was connected with a Pt wire) by a small brush to form a thick film [44]. Subsequently, the device was calcined at 500 °C for 2 h. It was aged for 7 days in order to enhance the stability of the gas sensors. To control the working temperature of the sensor, a Ni–Cr alloy coil was inserted as a heater into an aluminum oxide tube by adjusting the heating. The gas sensing properties of the sensors were measured by a static test system. During the testing, a given amount of target gases mixed with dry air were injected into an airtight chamber to obtain its desired concentrations. For an oxidizing gas, the response of the sensor is defined as S = Rg/Ra. For a reducing gas, the response was defined as S = Ra/Rg. Ra and Rg are the resistances of the sensor in air and target gas, respectively. The response and recovery times are defined as the time taken by the sensor to achieve 90% of the total resistance change in the case of adsorption and desorption, respectively.

3. Results and discussion

3.1. Structural and morphological characteristics

The X-ray diffractometry (XRD) analysis was performed to investigate the crystal structures and the effect of La^{3+} doping on the phase structures. The XRD patterns of pristine In_2O_3 and La–doped In_2O_3 hollow spheres are shown in Fig. 2a. All of the diffraction peaks could be indexed to cubic ferromanganese structure of In_2O_3, which were agreed well with the standard card from the Joint Committee on Powder Diffraction Standards card (JCPDS 71–2194). No other peak corresponding to lanthanum and lanthanum compound was observed in the XRD patterns of the doped nanomaterials, indicating that no impurity phase was formed. In addition, it was shown that the diffraction peaks became broader with the increased concentration of La dopant. According to Scherrer formula, the average crystallite sizes of S1, S2, S3, S4 were about 16.28, 11.31, 9.36, and 8.57 nm, respectively, which indicated that the addition of La could effectively prevent In_2O_3 crystallites from further growing up. To further evaluate the effect of La on the phase structures, the (222) and (400) diffraction peaks of these as-obtained simples were magnified and their comparison are showed in Fig. 2b. The high shifts (0.08°) of the peaks of the S3 to smaller 2θ

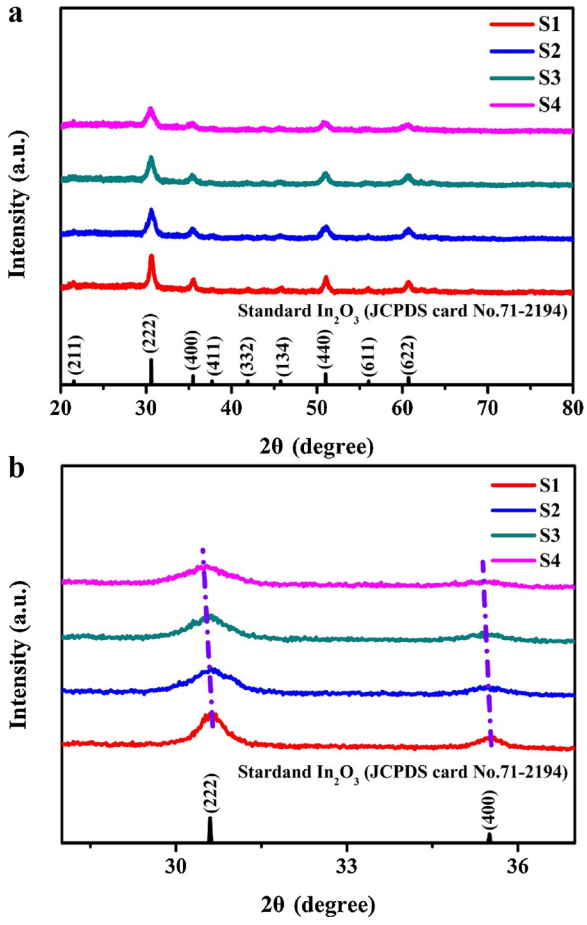

Fig. 2. (a) XRD patterns of La–doped In_2O_3 hollow microspheres with different molar ratios, (b) Comparison of (222) and (400) peaks from XRD patterns.

values were obviously observed compared with that of S1 sample. This could be ascribed to the difference between the radii of La^{3+} and In^{3+}. The radius of La^{3+} was 1.06 Å, which was larger than that of In^{3+} (0.81 Å) at the same coordination number. Thus, the diffraction peaks would shift to the left with increasing the La^{3+} addition amount. These results demonstrated the successful incorporation of lanthanum into In_2O_3 crystal lattice.

The morphological characteristics of the as-synthesized original and doped In_2O_3 with different La doping amount were observed by FESEM. The low-magnitude FESEM images were displayed in Fig. 3a–d, from which the uniform size spherical architecture and good dispersibility could be shown in Fig. 3a, whereas in Fig. 3b–d more uneven aggregates were observed with the increasing of La^{3+} addition amount. From the respective cracked In_2O_3 spherical architecture in the inset of Fig. 3a–d, the hollow structure of the obtained In_2O_3 could be verified. The observed single hollow spheres consist of many small nanoparticles. Meanwhile, the shell of In_2O_3 spherical architecture around 400 nm in thickness and the sizes of the S1, S2, S3, S4 were about 2.4 μm, 2.2 μm, 2.1 μm and 2.0 μm, respectively. It also could be exhibited that the grain boundary became more and more indistinct and the hollow spheres became more compact, which probably resulted from suppressed grain boundary migration and the increased energy barrier for grain growth.

In order to further study the lattice structure and more detailed structural features of La–doped In_2O_3 hollow microspheres, the transmission electron microscopy (TEM) images of S3 were displayed in Fig. 4. As seen in Fig. 4a, the synthesized samples exhibited homogeneous size and morphology. And the hollow structure of these microspheres could be shown clearly in Fig. 4b. In the high-magnification TEM images (HMTEM; Fig. 4c), the lattice plane could be obviously observed with the value of 0.357 nm, corresponding to the (220) plane of In_2O_3. The inset of Fig. 4c is the selected area electron diffraction pattern, in which a series of diffraction rings can be observed. It shows that the sample S3 is polycrystalline in nature. The energy dispersive X-ray spectroscopic (EDS) elemental mapping images (Fig. 4d–g) confirms the composition of the product and the spatial distribution of the elements. Obviously, In and O signals were detected as a hollow spherical structure, while La signals were detected in the whole hollow spherical region, which indicated the uniform distributions of La element over the whole sample S3.

3.2. Gas-sensing properties

In order to illuminate whether doping of La into In_2O_3 microstructures was an effective way to improve the device performance of the In_2O_3-based gas sensor, the gas sensing characteristics of the sensors based on all the samples were evaluated. It was well known that the operating temperature and the amount of dopant have great influence on the gas sensing properties of gas sensor. Fig. 5a showed the responses of the gas sensors based on the S1, S2, S3 and S4 to 10 ppm H_2S measured at different operating temperature from 175 to 300 °C aiming to determine the optimum operating temperature and the optimum doping amount. It is obvious that the response of all sensors rise with increasing the operating temperature until the value reached its maximum at an optimum operating temperature and then decreased with further increasing the operating temperature. The optimal operating temperature of every sample was 200 °C. Meanwhile, the gas response was greatly improved because of La doping. The gas responses of the sensors based on the S1, S2, S3 and S4 to 10 ppm H_2S at 200 °C were 3.7, 7.49, 17.8, and 10.7, respectively. Thus, 3.0 mol% La–doped In_2O_3 exhibited the highest response to 10 ppm H_2S, about 4.8 times higher than that of the original In_2O_3.

H_2S concentrations dependence of dynamic responses for the S1 and S3 at optimal operation temperature of 200 °C were revealed in Fig. 5b. The results indicated that the gas responses of these two sensors both increased as the H_2S concentration increased from 1 ppm to 200 ppm and the response enhanced significantly at the above detecting concentration of H_2S after the La–doped In_2O_3 hollow spheres. The responses of sensor based on S1 was 1.2, 1.8, 3.5, 8.3, 21.3, 32.2, 42.2 to 1, 5, 10, 20, 50, 100, 200 ppm H_2S, while the responses of sensor based on S3 were 2.48, 6.32, 18.2, 38.1, 50.3, 87.9, 111.9 to 1, 5, 10, 20, 50, 100, 200 ppm H_2S, respectively. Moreover, as shown in the inset of Fig. 5b, we could find that, compared with S1, the response of the sensor based on the S3 did not tend to saturation when the hydrogen sulfide concentration raised to 200 ppm, although the increasing trend slowed down with the increase of the hydrogen sulfide concentration. This indicated that the 3.0 mol% La–doped In_2O_3 hollow microspheres based gas sensor had a broad test range.

In terms of semiconductor gas sensors, selectivity was another important parameter. Fig. 6 revealed the selectivity of S1 and S3. The testing gases included H_2S, ethanol, acetone, formaldehyde, xylene, methanol and toluene. The testing conditions are 200 °C and 50 ppm. Obviously, the sensor based on S3 showed enhanced responses to all target gases in compare with S1, Particularly, its response to H_2S was 50.3, higher than other testing gases. The corresponding responses of S3 was 6.28, 5.75, 3.65, 2.23, 1.71 and 1.44 to ethanol, acetone, formaldehyde, xylene, methanol and toluene, respectively. Thus, we could say that S3 have an excellent selectivity toward H_2S over the other gases at 200 °C.

The response and recovery properties were additional major parameters for gas sensors. It was universally acknowledged that the recovery time is very long for hydrogen sulfide gas. The Fig. 7a showed the dynamic response and recover characteristics of sensors based on the S1 and S3 to 10 ppm H_2S at 200 °C. It could be seen that the resistance of the sensor changed immediately when H_2S was injected and

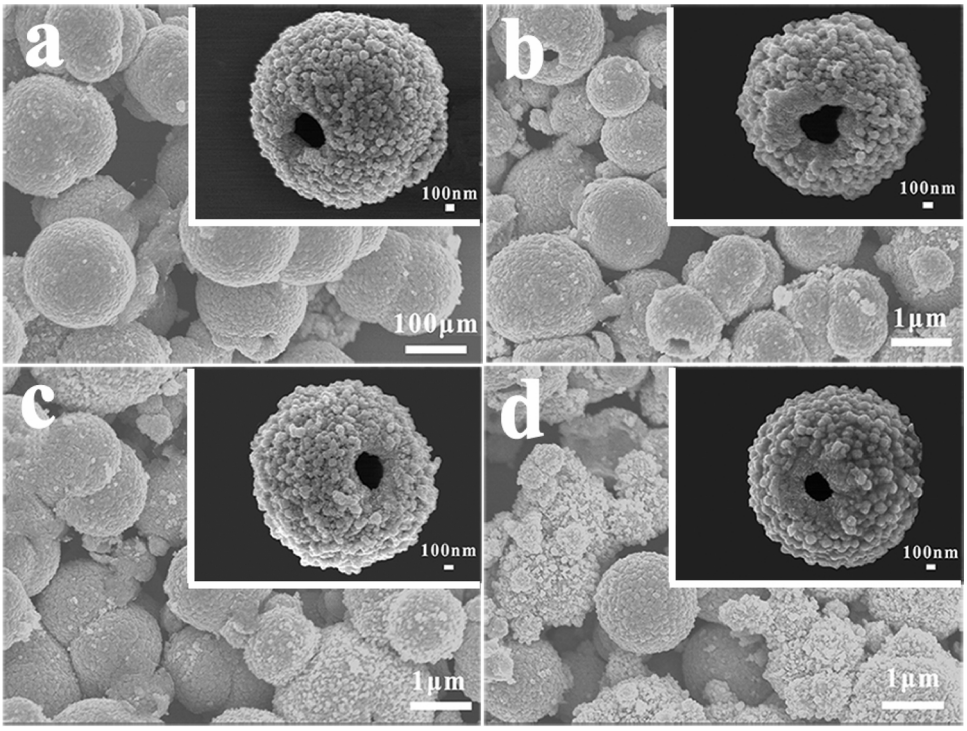

Fig. 3. FESEM images of (a) S1, (b) S2, (c) S3, (d) S4, the insets are high-magification images.

then reached a steady state quickly, the response time based on S3 and S1 were about 43 s and 178 s, respectively. It indicated that S3 had a great promotion on response time, which might result from the larger surface area of the hollow spheres provided sufficient active sites. However, when the sensors are put into air again, S3 and S1 would take a long time to return initial resistance value, which might caused by the difficult desorption of hydrogen sulfide gas in air. The four representative reversible cycles (shown in Fig. 7b) of H_2S response curve were carried out for S3. There was no clear floating in responses during the periods of cycle measurement to 10 ppm H_2S at 200 °C, which indicated its excellent repeatability and stability. Fig. 8 displayed the long term stability of the gas sensor S3 to 10 ppm H_2S at 200 °C for 30 days. The data was measured every three days. Notably, the response values just fluctuated 5% around 17.8, proving a relatively good stability of S3. According to the above measurement results, the excellent gas sensing characteristic for S3 might make it particularly attractive as a promising practical sensor.

3.3. Mechanism of the enhanced gas sensing performance

To date, the most widely accepted theory about semiconductor gas sensor is based on the change in the electrical conductivity caused by the interactions between the surface chemisorbed oxygen species and target gases [45]. Indium oxide is a typical n-type metal oxide semiconductor. When the In_2O_3 hollow microspheres were exposed to air, the oxygen molecules can be chemisorbed on the surface and captured electrons from the conduction band of In_2O_3 to form surface adsorbed oxygen species, such as O_2^-, O^-, and O^{2-} ions. Thus, an electron depletion layer on the surface of the In_2O_3 hollow microspheres was formed, giving rise to a high surface resistance via the loss of free electrons. When In_2O_3 hollow microspheres were exposed to H_2S, the following reactions will occur:

$$H_2S + 3O^{2-} \rightarrow H_2O + SO_2 + 6e^- \quad (1)$$

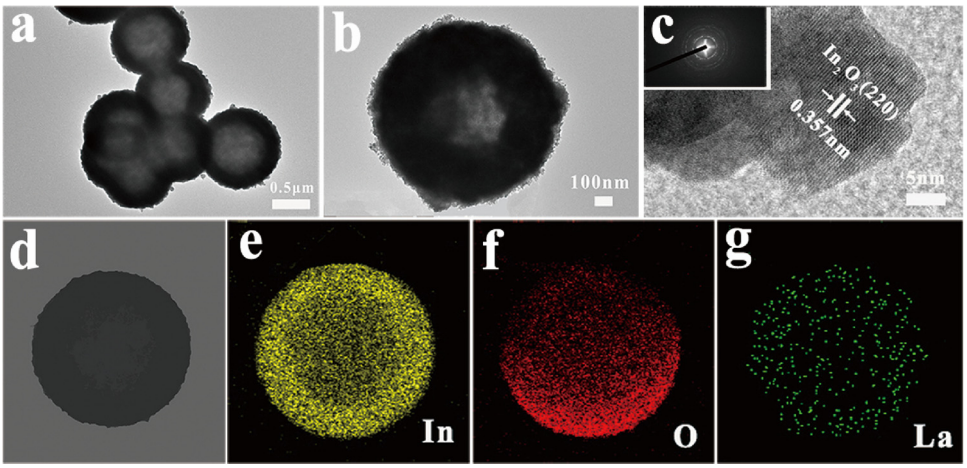

Fig. 4. (a)–(b) is TEM images patterns of S3. (c) is the HRTEM images of selected areas. The insets are selected area election diffraction (SAED) patterns. (d)–(g) are EDS elemental maps.

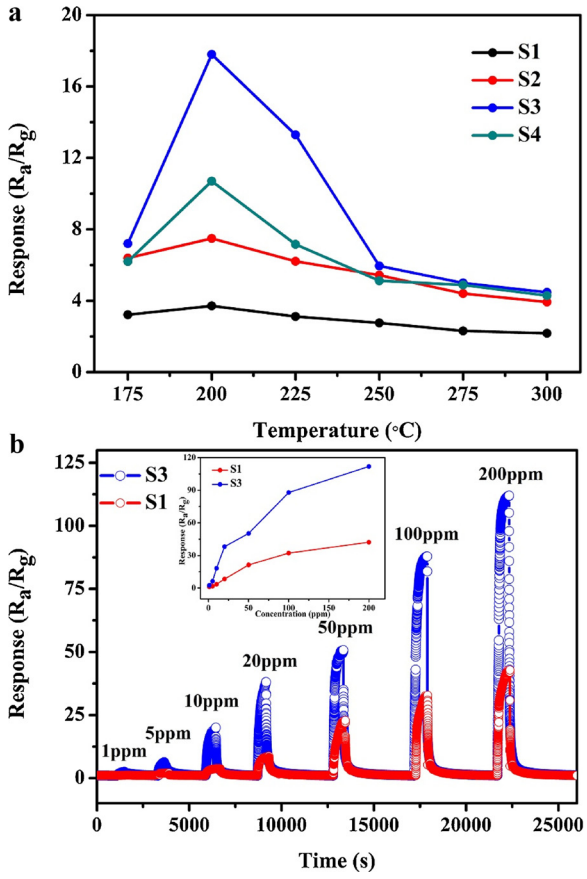

Fig. 5. (a) Response of sensors bases on S1, S2, S3 and S4 to 10 ppm H_2S as function of the operating temperature. (b) Response of sensors bases on S1 and S3 toward H_2S at different concentrations.

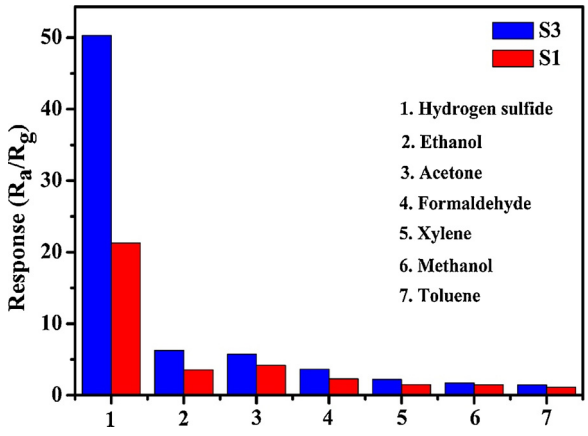

Fig. 6. Responses of the sensor based on S1 and S3 to 50 ppm various different gases at an operating temperature of 200 °C.

$$H_2S + 3O^- \rightarrow H_2O + SO_2 + 3e^- \quad (2)$$

The reactions will bring about releasing the electrons trapped in the ionized oxygen species back into the conduction band of In_2O_3, resulting in the decrease in the sensor resistance.

The enhancement of the gas response of the sensor base on the La–doped In_2O_3 hollow microspheres are likely to be attribute to the changes in distribution of different oxygen components, crystallite size and specific surface area. XPS analysis was performed at Fig. 9 in order to further explore the possible mechanism. Fig. 9a–d shows the high resolution scans of In 3d, La 3d, and O 1s, respectively. The In 3d spectrum (shown in Fig. 9a) has two strong peaks at binding energy of

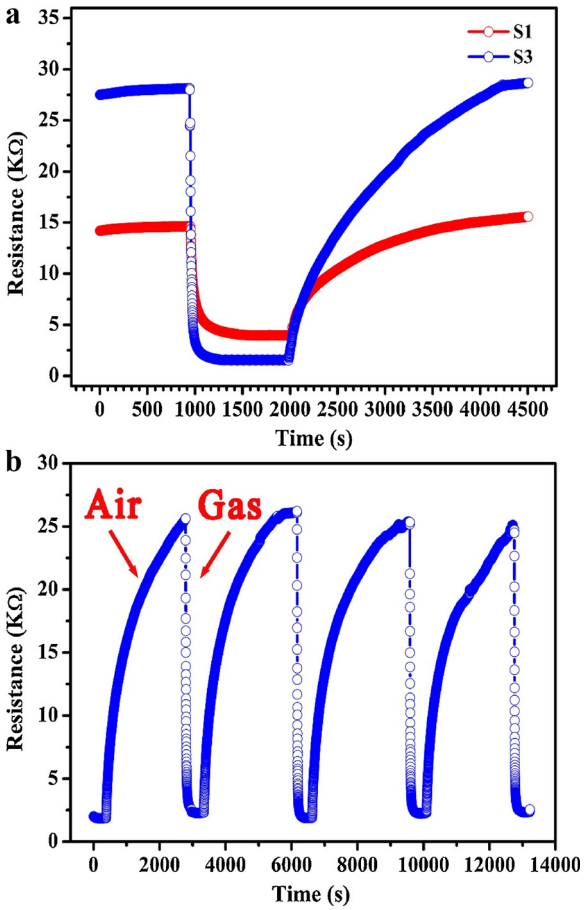

Fig. 7. (a) Dynamic response-recovery curve of S1 and S3 (a) four reversible cycles of S3 (b) to 10 ppm H_2S at 200 °C.

444.50 and 452.18 eV. They can be respectively indexed to the characteristic spin-orbit split states of In 3d5/2 and In $3d_{3/2}$, indicating a In oxidation state of +3. The XPS spectrum of La 3d electrons (displayed in Fig. 9b) could be divided into several Gaussian peaks. In this figure, the peaks at 835.20 eV and 838.86 eV were attributed to $La3d_{5/2}$, 852.46 eV and 855.84 eV are attributed to $La3d_{3/2}$. This further confirms the existence of La^{3+} ions in the sample. The O 1s peak was exhibited in Fig. 9c and d, in which it could be decomposed into three Gaussian peaks, indicating that there are significant differences between oxygen states on the surface of the samples. These three peaks were expressed as O_L, O_V, O_C, respectively. The O_L component was attributed to the lattice oxygen species, O_V component is associated with oxygen vacancy and the O_C is ascribed to chemisorbed oxygen in the surface of In_2O_3. They were located at 529.94 ± 0.4 eV (O_L), 530.60 ± 0.6 eV (O_V) and 531.94 ± 0.2 eV (O_C), respectively. The relative percentages of O_L, O_V, and O_C components were approximately 45.8%, 27.3% and 26.8% in S1, while they were 27.9%, 36.2% and 35.9% in S3. Obviously, with the increase of La doping concentration, the contents of O_V and O_C increase greatly. It had reported that gas sensitivity was closely related to the oxygen vacancy and chemisorbed oxygen on the surface of sensing material [46,47]. The augmentation of the O_V component could provide more active sites on the sensing material surface for gas adsorption reactions. The increase of O_C component means that more surface chemisorbed oxygen could participates in the redox reaction on the surface of In_2O_3 nanomaterials, which leads to larger change of the conductivity of the sensing material. The results also revealed that the La–doped In_2O_3 materials had the higher ability for adsorbing the ionized oxygen species. Therefore, the extraordinary ability of chemisorbing oxygen greatly contributes to the high-performance gas sensing toward H_2S gas.

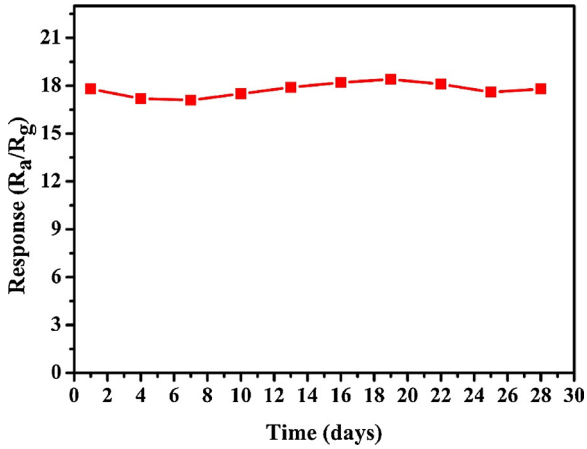

Fig. 8. The long-term stability of S3 to 10 ppm H_2S at 200 °C.

As we know, average crystallite sizes and specific surface areas might be also the key factors for the enhanced gas response [48]. To evaluate the specific surface areas of the samples, N_2 adsorption-desorption isotherms (shown in Fig. 10) are measured. The inset of Fig. 10 indicated that the nanoparticle pore sizes are around 10 nm, proving S1, S2, S3 and S4 were mesoporous materials. Nanoparticles were assembled into to a hollow sphere and pores are left between neighboring particles. The estimated specific surface areas of the S1, S2, S3 and S4 are about 33.73, 51.17, 55.95 and 39.71 $m^2 g^{-1}$, respectively. Obviously, when the concentration of La dopant is not too high, with the increasing of La doping concentration from S1 to S3, the specific surface area increases greatly. This means that the surface activity of the sensing material could be increased significantly, so that more oxygen can be absorbed and ionized owing to La doping. Meanwhile, the diffusion of the target gas and oxygen into the gas sensor body and the reaction between the target gas molecule and the chemisorbed oxygen ion also become easy. Therefore, the response to H_2S could increase with the increased specific surface area and S3 has the high sensitivity. However, for S4 with largest amount of La^{3+} content, its specific surface area and sensitivity were both decreased. Accordingly, the conclusion is that the larger specific surface area, the higher response was made. It is known that crystallite sizes also have an effect on the sensitivity. To clarify the relationship between crystallite sizes and specific surface area, their data are compared in Table 1. It could be seen that La doping leads to a decrease in the average grain size. As suggested by Noboru Yamazoe's work [49]. When the grain size was below or equal to twice of the Debye length, the response is inversely proportional to the size of the grain, that is to say, the smaller the size is, the more favorable it is to get a high response. This conclusion is consistent with the result of specific surface area. However, with the further decrease of crystallite size, the nanoparticles are apt to agglomerate forming a relatively dense spherical shell structure of In_2O_3 hollow spheres. In this way, the specific surface area decreased. Thus, the enhanced gas response might be partly explained by the decrease in crystallite size and the increase in specific surface area.

4. Conclusion

In summary, we successfully synthesized the pure and La–doped In_2O_3 hollow microspheres by one-step facile hydrothermal route. The results of a systematic and comparative gas sensing measurement indicated that the sensor based on the 3.0 mol% La–doped In_2O_3 has the significantly enhanced gas response to H_2S compared with the undoped, 1.0 mol%, and 5.0 mol% La–doped In_2O_3. Moreover, it has an excellent selectivity, good repeatability and outstanding long-term stability. The changes in distribution of different oxygen components, crystallite size and specific surface area caused by La doping could be responsible for the improvement of sensing properties. Hence, we could confirm that the La–doped In_2O_3 hollow microspheres is a promising strategy for designing and fabricating high performance H_2S sensor.

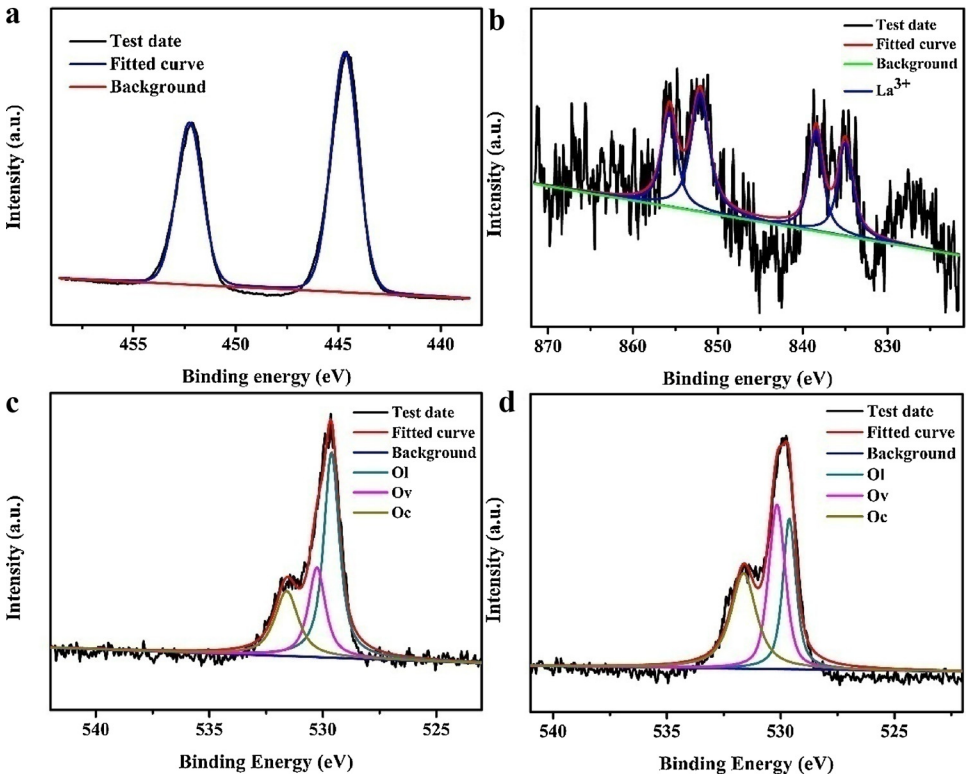

Fig. 9. XPS spectra of S1 and S3. (a) In 3d spectrum of S3, (b) La 3d spectrum of S3, (c) O 1s spectrum of S1, (c) O 1s spectrum of S3.

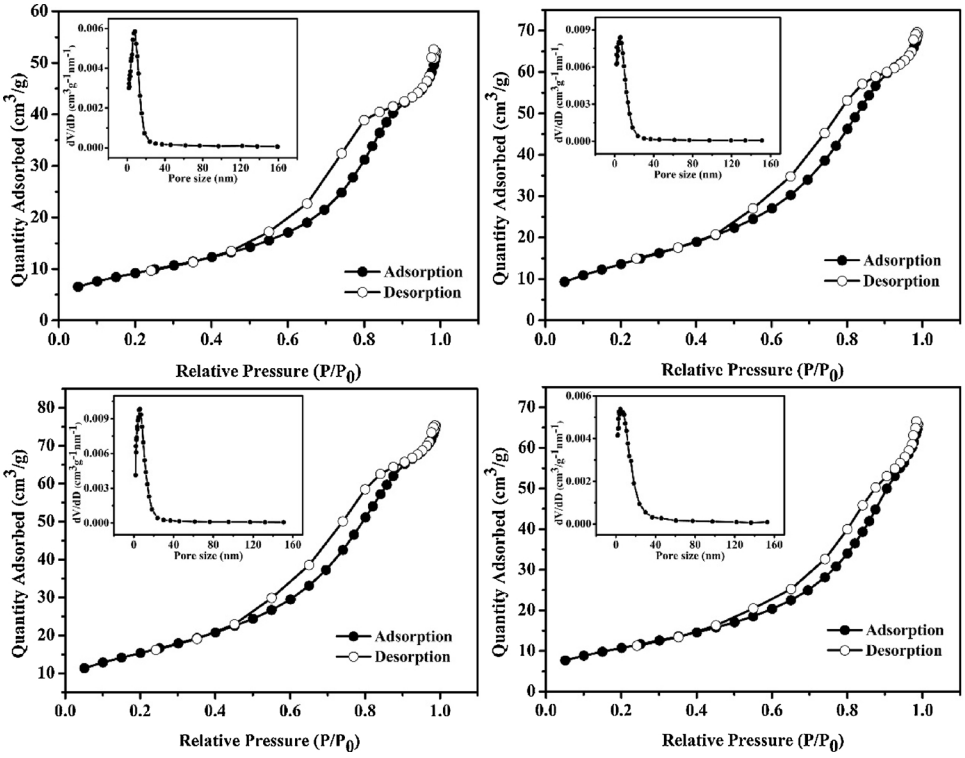

Fig. 10. N_2 adsorption-desorption isotherms of the (a) S1, (b) S2, (c) S3 and (d) S4.

Table 1
Comparison of the average crystallite sizes and specific surface areas of the S1, S2, S3 and S4.

Sample name	S1	S2	S3	S4
Average crystallite size (nm)	16.28	11.31	9.36	8.57
Specific surface area ($m^2 g^{-1}$)	33.73	51.17	55.95	39.71

Acknowledgements

This work is supported by National Key Research and Development Program of China (No. 2016YFC0201002), National Nature Science Foundation of China (No. 6152010600), National High-Tech Research and Development Program of China (863 Program, No. 2014AA06A505). High level scientific and technological innovation team of Jilin University (2017TD-07).

References

[1] S.L. Bai, K.W. Zhang, J.H. Sun, D.F. Zhang, Polythiophene-WO_3 hybrid architectures for low-temperature H_2S detection, Sens. Actuators B Chem. 197 (2014) 142–148.
[2] J. Ma, Y.K. Liu, H. Zhang, P. Ai, Room temperature ppb level H_2S detection of a single Sb-doped SnO_2 nanoribbon device, Sens. Actuators B Chem. 216 (2015) 72–79.
[3] A. Samokhvalov, B.J. Tatarchuk, Characterization of active sites, determination of mechanisms of H_2S, COS and CS_2 sorption and regeneration of ZnO low temperature sorbents: past, current and perspectives, Phys. Chem. 13 (2011) 3197–3209.
[4] S.S. Badadhe, I.S. Mulla, H_2S gas sensitive indium-doped ZnO thin films: preparation and characterization, Sens. Actuators B Chem. 143 (2009) 164–170.
[5] J.W. Yoon, Y.J. Hong, Y.C. Kang, J.H. Lee, High performance chemiresistive H_2S sensors using Ag-loaded SnO_2 yolk-shell nanostructures, RSC Adv. 4 (2014) 16067–16074.
[6] H.S. Woo, C.H. Kwak, I.D. Kim, J.H. Lee, Highly selective, sensitive, and reversible H2S sensors using Mo-doped ZnO nanowire networks, J. Mater. Chem. A Mater. Energy Sustain. 2 (2014) 6412–6418.
[7] X. Liang, Y. He, F. Liu, B. Wang, T. Zhong, B. Quan, G. Lu, Solid-state potentiometric H_2S sensor combining NASICON with Pr_6O_{11}-doped SnO_2 electrode, Sens. Actuators B Chem. 125 (2007) 544–549.
[8] Y. Guan, C. Yin, X. Cheng, X. Liang, Q. Diao, H. Zhang, G. Lu, Sub-ppm H_2S sensor based on YSZ and hollow balls $NiMn_2O_4$ sensing electrode, Sens. Actuators B Chem. 193 (2014) 501–508.
[9] N. Joshi, V. Saxena, A. Singh, S.P. Koiry, A.K. Debnath, M.M. Chehimi, D.K. Aswal, S.K. Gupta, Flexible H_2S sensor based on gold modified polycarbazole films, Sens. Actuators B Chem. 200 (2014) 227–234.
[10] A. Mekki, N. Joshi, A. Singh, Z. Salmi, P. Jha, P. Decorse, S. Truong, R. Mahmoud, M.M. Chehimi, D.K. Aswal, S.K. Gupta, H_2S sensing using in situ photopolymerized polyaniline-silver nanocomposite films on flexible substrates, Org. Electron. 15 (2014) 71–81.
[11] Y. Shen, B. Zhang, X. Cao, D. Wei, J. Ma, L. Jia, S. Gao, B. Cui, Y. Jin, Microstructure and enhanced H_2S sensing properties of Pt-loaded WO_3 thin films, Sens. Actuators B Chem. 193 (2014) 273–279.
[12] Y. Chen, F. Meng, H. Yu, C. Zhu, T. Wang, P. Gao, Q. Ouyang, Sonochemical synthesis and ppb H_2S sensing performances of CuO nanobelts, Sens. Actuators B Chem. 176 (2013) 15–21.
[13] J. Xu, X. Wang, J. Shen, Hydrothermal synthesis of In_2O_3 for detecting H_2S in air, Sens. Actuators B Chem. 115 (2006) 642–646.
[14] N.S. Ramgir, S.K. Ganapathi, M. Kaur, N. Datta, K.P. Muthe, D.K. Aswal, S.K. Gupta, J.V. Yakhmi, Sub-ppm H_2S sensing at room temperature using CuO thin films, Sens. Actuators B Chem. 151 (2010) 90–96.
[15] J.Z. Zhen Zhang, Y. Yan, Synthesis of biomorphic tube-like CuO using pomelo white flesh as biotemplate and its sensing properties over H_2S at room temperature, J. Mater. Sci. 52 (2017) 13711–13718.
[16] D. Vuong, G. Sakai, K. Shimanoe, N. Yamazoe, Hydrogen sulfide gas sensing properties of thin films derived from SnO_2 sols different in grain size, Sens. Actuators B Chem. 105 (2005) 437–442.
[17] P. Sun, X. Zhou, C. Wang, B. Wang, X.M. Xu, G.Y. Lu, One-step synthesis and gas sensing properties of hierarchical Cd-doped SnO_2 nanostructures, Sens. Actuators B Chem. 190 (2014) 32–39.
[18] Y. Wang, F. Kong, B. Zhu, S. Wang, S. Wu, W. Huang, Synthesis and characterization of Pd-doped –Fe_2O_3 H_2S sensor with low power consumption, Mater. Sci. Eng. B 140 (2007) 98–102.
[19] K. Tian, X.X. Wang, Z.Y. Yu, H.Y. Li, X. Guo, Hierarchical and hollow Fe_2O_3nanoboxes derived from metal – organic frameworks with excellent sensitivity to H_2S, ACS Appl. Mater. Interfaces 9 (2017) 29669–29676.
[20] S.L. Bai, K.W. Zhang, J.H. Sun, D.F. Zhang, R.X. Luo, D.Q. Li, C.C. Liu, Polythiophene – WO_3 hybrid architectures for low-temperature H_2S detection, Sens. Actuators B Chem. 197 (2014) 142–148.
[21] J.J. Shi, Z.X. Cheng, L.P. Gao, Y. Zhang, J.Q. Xu, H.B. Zhao, Facile synthesis of reduced graphene oxide/hexagonal WO_3 nanosheets composites with enhanced H_2S sensing properties, Sens. Actuators B Chem. 230 (2016) 736–745.
[22] Y.Y. Wang, G.T. Duan, Y.D. Zhu, H.W. Zhang, Z.K. Xu, Z.F. Dai, W.P. Cai, Room temperature H_2S gas sensing properties of In_2O_3 micro/nanostructured porous thin film and hydrolyzation-induced enhanced sensing mechanism, Sens. Actuators B Chem. 228 (2016) 74–84.
[23] W.W. Chen, Y.K. Liu, Z.J. Qin, Y.M. Wu, S.H. Li, P. Ai, A single Eu-doped In_2O_3 nanobelt device for selective H_2S detection, Sensors 15 (2015) 29950–29957.
[24] B.X. Xiao, F. Wang, C.B. Zhai, P. Wang, C.H. Xiao, Facile synthesis of In_2O_3

nanoparticles for sensing properties at low detection temperature, Sens. Actuators B Chem. 235 (2016) 251–257.
[25] Y.J. Li, H.R. Yang, J. Tian, X.L. Hu, H.Z. Cui, Synthesis of In_2O_3 nanoparticle/TiO_2 nanobelt heterostructures for near room temperature ethanol sensing, RSC Adv. 7 (2017) 11503–11509.
[26] C. Li, D.H. Zhang, S. Han, X.L. Liu, T. Tang, C.W. Zhou, Diameter-controlled growth of single-crystalline In_2O_3 nanowires and their electronic properties, Adv. Mater. 15 (2003) 143–146.
[27] A.U. Rehman, J.W. Zhang, J. Zhou, K. Kan, L. Li, K.Y. Shi, Synthesis of mesoporous K_2O-In_2O_3 nanowires and NO_x gas sensitive performance study in room temperature, Microporous Mesoporous Mater. 240 (2017) 50–56.
[28] Z.X. Cheng, X.B. Dong, Q.Y. Pan, J.C. Zhang, X.W. Dong, Preparation and characterization of In_2O_3 nanorods, Mater. Lett. 60 (2006) 3137–3140.
[29] W.C. Fang, Y. Yang, H. Yu, X.T. Dong, R.H. Wang, An In_2O_3 nanorod-decorated reduced graphene oxide composite as a high-response NO_x gas sensor at room temperature, New J. Chem. 41 (2017) 7517–7523.
[30] R.J. Ma, X. Zhao, X.X. Zou, G.D. Li, Enhanced formaldehyde sensing performance at ppb level with Pt-doped nanosheet-assembled In_2O_3 hollow microspheres, J. Alloys Compd. 732 (2018) 863–870.
[31] L. Sun, W.C. Fang, Y. Yang, H. Yu, T.T. Wang, Highly active and porous single-crystal In_3O_3 nanosheet for NO_x gas sensor with excellent response at room temperature, RSC Adv. 7 (2017) 33419–33425.
[32] B.X. Xiao, D.X. Wang, S.L. Song, C.B. Zhai, F. Wang, M.Z. Zhang, Fabrication of mesoporous In_2O_3 nanospheres and their ultrasensitive NO_2 sensing properties, Sens. Actuators B Chem. 248 (2017) 519–526.
[33] B.X. Xiao, Q. Zhao, D.X. Wang, G.S. Ma, M.Z. Zhang, Facile synthesis of nanoparticle packed In_2O_3 nanospheres for highly sensitive NO_2 sensing, New J. Chem. 41 (2017) 8530–8535.
[34] D.D. Wei, Z.S. Huang, L.W. Wang, X.H. Chuai, S.M. Zhang, G.Y. Lu, Hydrothermal synthesis of Ce-doped hierarchical flower-like In_2O_3 microspheres and their excellent gas-sensing properties, Sens. Actuators B Chem. 255 (2018) 1211–1219.
[35] X.M. Xu, H.J. Zhang, X.L. Hu, P. Sun, Y.S. Zhu, Hierarchical nanorod-flowers indium oxide microspheres and their gas sensing properties, Sens. Actuators B Chem. 227 (2016) 547–553.
[36] X.Y. Kou, N. Xie, F. Chen, T.S. Wang, L.L. Guo, C. Wang, Superior acetone gas sensor based on electrospun SnO_2 nanofibers by Rh doping, Sens. Actuators B Chem. 256 (2018) 861–869.
[37] X.B. Hu, Z.G. Zhu, C. Chen, T.Y. Wen, Highly sensitive H_2S gas sensors based on Pd-doped CuO nanoflowers with low operating temperature, Sens. Actuators B Chem. 253 (2017) 809–817.
[38] J. Shu, Z.L. Qiu, S.Z. Lv, K.T. Zhang, D.P. Tang, Cu^{2+}-doped SnO_2 Nanograin/Polypyrrole nanospheres with synergic enhanced properties for ultrasensitive room-temperature H_2S gas sensing, Anal. Chem. 89 (2017) 11135–11142.
[39] J. Sukunta, A. Wisitsoraat, A. Tuantranont, S. Phanichphant, C. Liewhiran, Highly-sensitive H_2S sensors based on flame-made V-substituted SnO_2 sensing films, Sens. Actuators B Chem. 242 (2017) 1095–1107.
[40] X.L. Xu, Y. Chen, S.Y. Ma, W.Q. Li, Y.Z. Mao, Excellent acetone sensor of La-doped ZnO nanofibers with unique bead-like structures, Sens. Actuators B Chem. 213 (2015) 222–233.
[41] J.Q. He, J. Yin, D. Liu, L.X. Zhang, F.S. Cai, L.J. Bie, Enhanced acetone gas-sensing performance of La_2O_3-doped flowerlike ZnO structure composed of nanorods, Sens. Actuators B Chem. 182 (2013) 170–175.
[42] V.D. Kapse, S.A. Ghosh, G.N. Chaudhari, F.C. Raghuwanshi, D.D. Gulwade, H_2S sensing properties of La-doped nanocrystalline In_2O_3, Vacuum 83 (2009) 346–352.
[43] V.D. Kapse, S.A. Ghosh, F.C. Raghuwanshi, S.D. Kapse, Enhanced H_2S sensing characteristics of La-doped In_2O_3: effect of Pd sensitization, Sens. Actuators B Chem. 137 (2009) 681–686.
[44] X.W. Li, P. Sun, T.L. Yang, J. Zhao, Z.Y. Wang, W.N. Wang, Y.P. Liu, G.Y. Lu, Template-free microwave-assisted synthesis of ZnO hollow microspheres and their application in gas sensing, CrystEngComm 15 (2013) 2949–2955.
[45] X.M. Gao, Y. Sun, C.L. Zhu, C.Y. Li, Q.Y. Ouyang, Y.J. Chen, Highly sensitive and selective H_2S sensor based on porous $ZnFe_2O_4$ nanosheets, Sens. Actuators B Chem. 246 (2017) 662–672.
[46] L.P. Gao, F.M. Ren, Z.X. Cheng, Y. Zhang, Q. Xiang, J.Q. Xu, Porous corundum-type In_2O_3 nanoflowers: controllable synthesis, enhanced ethanol-sensing properties and response mechanism, CrystEngComm 17 (2015) 326.
[47] C. Wang, X. Cui, J. Liu, X. Zhou, X. Cheng, P. Sun, X. Hu, X. Li, J. Zheng, G. Lu, Design of superior ethanol gas sensor based on Al-doped NiO nanorod-flowers, ACS Sens. 1 (2016) 131–136.
[48] C. Wang, J.Y. Liu, Q.Y. Yang, P. Sun, Y. Gao, F.M. Liu, J. Zheng, G.Y. Lu, Ultrasensitive and low detection limit of acetone gas sensor based on W-doped NiO hierarchical nanostructure, Sens. Actuators B Chem. 220 (2015) 59–67.
[49] N. Yamazoe, G. Sakai, K. Shimanoe, Oxide semicomductor gas sensors, Catal. Surv. Asia 7 (2003) 63–75.

Dongdong Wei received the BS degree in Changchun University of Science and Technology in 2016. He is currently studying for his MS degree in College of Electronic Science and Engineering, Jilin University, China. His research interests include the synthesis of In_2O_3 functional materials and their applications in gas sensors.

Wenhao Jiang received the BS degree in Changchun University of Science and Technology in 2017. He is currently studying for his MS degree in College of Electronic Science and Engineering, Jilin University, China.

Hongyu Gao received the BS degree in Department of Electronic Science and Engineering in 2016. He is currently studying for his MS degree in College of Electronic Science and Engineering, Jilin University, China.

Xiaohong Chuai received the Ph. D degree in inorganic nonmetal science from Beijing University of science in 2001, and then worked at the school of Electronic Science and engineering, Jilin University. Now, she is engaged in the synthesis and characterization of the semiconducting functional materials and gas sensors.

Fengmin Liu received the BE degree in Department of Electronic Science and Technology in 2000. She received his Doctor's degree in College of Electronic Science and Engineering at Jilin University in 2005. Now she is a professor in Jilin University, China. Her current research is preparation and application of semiconductor oxide, especial in gas sensor and solar cell.

Fangmeng Liu received his PhD degree in 2017 from College of Electronic Science and Engineering, Jilin University, China. Now he is a lecturer of Jilin University, China. His current research interests include the application of functional materials and development of solid state electrochemical gas sensor and flexible device.

Peng Sun received his PhD degree from the Electronics Science and Engineering department, Jilin University, China in 2014. Now, he is engaged in the synthesis and characterization of the semiconducting functional materials and gas sensors.

Xishuang Liang received the B. Eng. degree in Department of Electronic Science and Technology in 2004. He received his Doctor's degree in College of Electronic Science and Engineering at Jilin University in 2009. Now he is an associate professor of Jilin University, China. His current research is solid electrolyte gas sensor.

Yuan Gao received her PhD degree from Department of Analytical Chemistry at Jilin University in 2012. Now she is an associate professor in Jilin University, China. Her current research is focus on the preparation and application of graphene and semiconductor oxide, especial in gas sensor and biosensor.

Xu Yan received his M.S. degree in 2013 from Nanjing Agricultural University. He joined the group of Prof. Xingguang Su at Jilin University and received his Ph.D. degree in June 2017. Since then, he did postdoctoral work with Prof. Geyu Lu. Currently, his research interests mainly focus on the development of the functional nanomaterials for chem/bio sensors.

Geyu Lu received the BS degree in electronic sciences in 1985 and the MS degree in 1988 from Jilin University in China and the Dr Eng degree in 1998 from Kyushu University in Japan. Now he is a professor of Jilin University, China. Now, he is interested in the development of functional materials and chemical sensors received the B. Eng. Degree in Department of Electronic Science and Technology in 2004. He received his Doctor's degree in College of Electronic Science and Engineering at Jilin University in 2009. Now he is a lecturer of Jilin University, China. His current research is solid electrolyte gas sensor.